applied sciences

MDPI

Article

Analysis of Six Active Power Control Strategies of Interconnected Grids with VSC-HVDC

Sungyoon Song [1], Minhan Yoon [2] and Gilsoo Jang [1,*]

[1] School of Electrical Engineering, Korea University, Anam-ro, Sungbuk-gu, Seoul 02841, Korea; blue6947@korea.ac.kr

[2] Department of Electrical Engineering, Tongmyong University, Sinseon-ro, Nam-gu, Busan 48520, Korea; minhan.yoon@gmail.com

* Correspondence: gjang@korea.ac.kr; Tel.: +82-010-3412-2605

Received: 29 November 2018; Accepted: 31 December 2018; Published: 6 January 2019

Abstract: In this paper, the generator angle stability of several active power control schemes of a voltage-source converter (VSC)-based high-voltage DC (HVDC) is evaluated for two interconnected AC systems. Excluding frequency control, there has been no detailed analysis of interconnected grids depending upon the converter power control, so six different types of active power control of the VSC-HVDC are defined and analyzed in this paper. For each TSO (transmission system operator), the applicable schemes of two kinds of step control and four kinds of ramp-rate control with a droop characteristic are included in this research. Furthermore, in order to effectively evaluate the angle stability, the Generators-VSC Interaction Factor (GVIF) index is newly implemented to distinguish the participating generators (PGs) group which reacts to the converter power change. As a result, the transient stabilities of the two power systems are evaluated and the suitable active power control strategies are determined for two TSOs. Simulation studies are performed using the PSS®E program to analyze the power system transient stability and various active power control schemes of the VSC-HVDC. The results provide useful information indicating that the ramp-rate control shows a more stable characteristic than the step-control for interconnected grids; thus, a converter having a certain ramp-rate slope similar to that of the other generator shows more stable results in several cases.

Keywords: grid-interconnection; active power control strategies; transient stability; GVIF index; angle spread; VSC-HVDC

1. Introduction

Presently, renewable energy resources are considered a best practice in the response to global warming, and these power resources are concentrated in remote areas in order to effectively generate power. However, several instability issues arising from uneven large power generation requires TSOs (transmission system operators) to complement the grid structure [1]. Moreover, based on References [2–4], grid interconnection is emerging as an effective alternative for solving stability problems. For example, Nordic power systems in which several grids are interconnected by AC or DC links have increasingly accepted renewable energy resources, and have updated their hourly power exchange clauses [5]. This additional effort has led to the mitigation of several instability issues caused by uneven power generation, and many research works have also reported that renewable energy resources have become more accepted in many other countries [6].

In order to interconnect two different power systems, there are two options for TSOs: AC or DC lines. Nowadays, grid interconnection using an AC transmission line has a problem that increases the system complexity from the operation point of view, and may adversely decrease the system reliability. In fact, large blackouts have clearly confirmed that the close coupling of the neighboring

systems might also include the risk of uncontrolled cascading effects in large and heavily loaded systems [7]. Furthermore, the AC system is vulnerable to sub-sea transmission connections and long interconnection; thus, the DC system, which has the advantage of high controllability, has been widely deployed for grid interconnection projects [8]. Considering the grid strength as the SCR (short circuit ratio) at each point, it is well known that the LCC (line commutated converter)-based high-voltage DC (HVDC) is restricted in that the converter cannot work properly if the connected AC system is weak [9]. Conservatively, in the case of AC systems with an SCR lower than 1.5, synchronous condensers have to be installed so as to increase the SCR of the AC system. In addition, the reactive power should be compensated depending upon the power sent, which reduces the simplicity of controllability in LCCs. The voltage-source converter (VSC)-HVDC has similar stability issues; however, it offers significant advantages such as high controllability, reliability, and small size. Benefiting from the significant technical advances in insulated gate bipolar transistors (IGBT), the VSC has become a competitive alternative to the LCC, so the VSC-HVDC is more commonly deployed nowadays. In the VSC system, two main stability issues have generally been presented in detail to date:

(1) Operation region of the VSC-HVDC

The reactive power of the VSC-HVDC can be limited according to the AC grid voltage and the equivalent impedance. In addition, the DC voltage control and PLL (Phase-Locked Loop) can restrict the power angle to approximately 51° for a stable operation without the support of the dynamic reactive power [10]. In order to obtain an improved power transfer capability from the VSC-HVDC, the X/R ratio (the ratio of the system reactance to the system resistance) and the impedance angle must be considered. Therefore, the SCR index representing the grid strength is an important factor from the perspective of the capability region.

(2) Dynamic performance of the VSC-HVDC

In previous studies on the relationship between the PLL and the VSC-HVDC, many authors have mentioned that a converter with large PLL gains that is connected to a weak AC grid (2 < SCR) is prone to instabilities when subjected to a disturbance [11]. This is because the PLL that is used for the angle-reference generation can easily generate an unstable eigenvalue with high proportional gains. The AC voltage phase is highly sensitive to the d and q current injections of the converter in a weak grid. Detailed results have been described in a few references [12,13].

However, the stability issues mentioned above can be resolved by the robust compensator design mentioned by many authors [12–15]. The robust PI (Proportional and Integral) parameters, feedforward controllers, and adjusted PLL parameters enable the stable operation of VSC-HVDC, and the damping condition which occurs at a certain frequency range can be mitigated. Therefore, in this work, the VSC-HVDC system is deployed without considering the small signal stability issues, and the main contribution of this paper is to analyze the impact of six active power control strategies on the generator angle stability of two interconnected grids.

Excluding the contingency event, the fixed power control for two grids is commonly used to lessen the operation burdens of TSOs. However, during a contingency event, the power should be adjusted to provide grid services such as frequency support or transient stability support. According to the previous works related to VSC control for grid service, Reference [16] demonstrated the AC transmission emulation control strategy, which acts like an AC line when a contingency event occurs. It is able to mitigate the possible overloading of adjacent AC transmission, and maintain power balance between metropolitan regions. However, the transferred power is not exactly estimated since the output power is varied depending upon contingency event types; thus, it is not suitable for interconnected grids since there is a clear exchange clause in their agreement. In Reference [17], the flexible operation of the generator tripping scheme was achieved without a large decelerating energy as the generators trip, and it was confirmed that a simple converter control strategy that transfers the maximum power reserve instantly to the fault area surely contributes to the stability of the

AC network. However, this paper only addressed one kind of step control. In References [18,19], the DC voltage droop, local frequency control, and weighted-average frequency control are compared in detail; however, this analysis was performed in an embedded MTDC (multi-terminal DC) environment. In References [20,21], the kinds of frequency–power modulation control strategies for the converter to enhance the system transient stability are introduced. As can be observed, there has been no detailed analysis of interconnected grids depending upon the several converter power control schemes in a point-to-point environment. Therefore, in this paper, two step control and four ramp-rate control scenarios are specifically defined, and then simulated to provide useful feasibility studies results for grid operators.

A dynamic control model of the VSC-HVDC is developed written by Fortran language in the PSS®E program (Power Transmission System Planning Software), and the ideal averaged equivalent VSC model is used. The MMC (modular multilevel converter) is not used since the AC system stability is the major observation target. To perform this analysis, the GVIF index, meaning the Generators-VSC Interaction Factor, is newly defined in Section 2. In Section 3, the introduction of the VSC-HVDC model serves to illustrate the configuration of the active power controller. In addition, six active power control strategies are defined in Section 4. Lastly, a simulation of the transient stability regarding the control schemes is performed.

2. Identify PGs (Participating Generators) with the GVIF Index

As shown in Figure 1, areas 1 and 2 are interconnected by a VSC-HVDC link. The initial DC power direction is from area 1 to area 2, so the converter is used to provide auxiliary service for area 2. This grid structure may be in the form of an interconnection link between countries or between regions [18]. If multiple generators are connected in parallel to each area, it is difficult to detect which generator contributes to incremental power according to the converter power change. The TSOs must determine which generators respond to the converter control, and this process is needed to distinguish the participating generators (PGs) group.

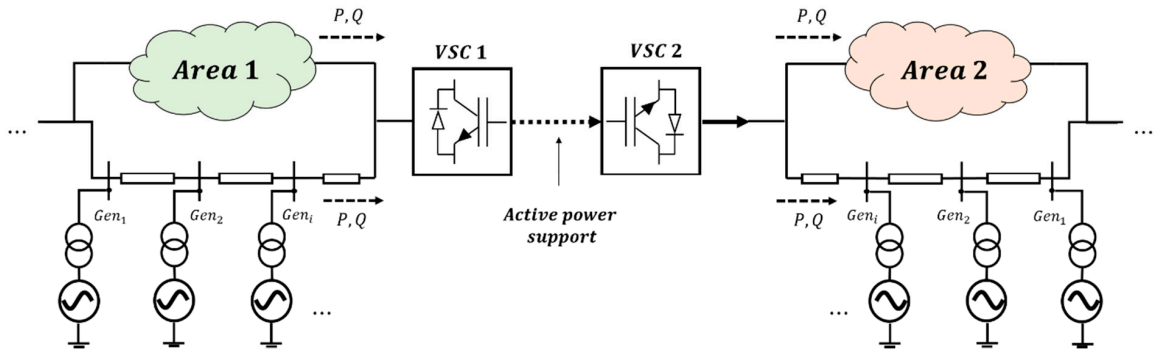

Figure 1. Two interconnected grids with a voltage-source converter (VSC)-based high-voltage DC (HVDC).

A traditional synchronous generator consists of a governor and a prime mover to support frequency regulation. The simplified first-order differential equation of the dynamic generator model is shown in Equations (1) and (2), where P_v is the valve position of the governor; P_{ref} is the power reference of governor; R is the droop value; P_m is the prime mover output power; and T_G and T_P are the time constants of the governor and prime mover, respectively [22].

$$\frac{d\Delta P_v}{dt} = -\frac{\Delta P_v}{T_G} + \frac{\Delta P_{ref}}{T_G} - \frac{1}{T_G R}\Delta f. \quad (1)$$

$$\frac{d\Delta P_m}{dt} = -\frac{\Delta P_m}{T_P} + \frac{\Delta P_v}{T_P}. \quad (2)$$

Based on Equations (1) and (2), the generators react to grid frequency change as Δf. If all generators have the same frequency droop value, an individual generator increases in the same MW power in a liner decrease in speed corresponding to the percent droop selected and no-load frequency. However, in the real grid operation, the frequency measurement result as Δf is slightly different at each region at the same time; thus, the ΔP_v and ΔP_m were made unlike the expected values. During the dynamic state, the generator output power is mainly determined by the droop value as R, but it is also related to the distance to the point at which the frequency change occurs. As a result, the approximate incremental output of each generator with the droop slope can be estimated, but it is difficult to derive the exact incremental power from each generator. In order to consider both the governor droop value and the electrical distance between the generators and the converter, the new grouping index, referred to as the Generators-VSC Interaction Factor (GVIF) to select the PGs is implemented as follows.

$$GVIF_{i,j} = \frac{\Delta P_i}{\Delta P_j}. \tag{3}$$

where bus i is the generator bus connected in area 1. Bus j is the VSC-HVDC bus, and as we know, the multi-infeed HVDC system has several bus positions as $j \geq 2$. The GVIF is the dynamic active power change of bus j over the active power change of bus i. When the active power change ΔP_j is 1%, the active power change ratio of bus i is the GVIF. If the generators have the same frequency–power droop value, the electrical distance is the main factor impacting the GVIF since the frequency measurement results are slightly different at each region. Thus, using the GVIF, the frequency measurement result errors could be corrected on each generator output. In the steady-state condition, since the frequency change point is always the converter bus as bus j, the generators with a high GVIF index could be considered to be closer to the converter or to have a high droop value. The generator which has a zero value of GVIF does not participate in the incremental power generation. In this paper, we define the generators with GVIF > 0 as PGs, and the angle stabilities of all PGs are evaluated by the general transient stability index as angle spread in Section 5.

3. Active Power Controller Design of VSC-HVDC

The schematic diagram of the VSC-HVDC is illustrated in Figure 2. The widely used vector controller is applied in the VSC. Let the converter side impedance be simply modeled as a series-connected three phase inductor and resistor, and the AC grid in the *abc* frame is:

$$\begin{bmatrix} v_1^d \\ v_1^q \end{bmatrix} - \begin{bmatrix} v_2^d \\ v_2^q \end{bmatrix} = R \begin{bmatrix} i_d \\ i_q \end{bmatrix} + L \frac{d}{dt} \begin{bmatrix} i_d \\ i_q \end{bmatrix} - \begin{bmatrix} -\omega L i_q \\ \omega L i_d \end{bmatrix}, \tag{4}$$

where the v_2 is the voltage at PCC and v_1 is the voltage at the converter. In addition, R and L are the resistance and inductance, respectively, and i is the current flowing to the AC grid. Filter components prevent the generation of harmonic current by the converter, and they also affect the stability between the AC grid and the VSC.

The reference voltage generated by the inner current control loop is transformed back into the *abc* frame and used for Pulse With Modulation (PWM) to produce the desired converter three-phase voltage. The voltage reference sent to the PWM is represented by:

$$\begin{bmatrix} \Delta v_2^d \\ \Delta v_2^q \end{bmatrix} = - \begin{bmatrix} A_d(s) \\ A_q(s) \end{bmatrix} \begin{bmatrix} \Delta i_{d,ref} - \Delta i_d \\ \Delta i_{q,ref} - \Delta i_q \end{bmatrix} + \omega L \begin{bmatrix} -\Delta i_q \\ \Delta i_d \end{bmatrix} + \begin{bmatrix} v_1^d \\ v_1^q \end{bmatrix}, \tag{5}$$

where $A_d(s)$ *and* $A_q(s) = \frac{k_p s + k_i}{s}$.

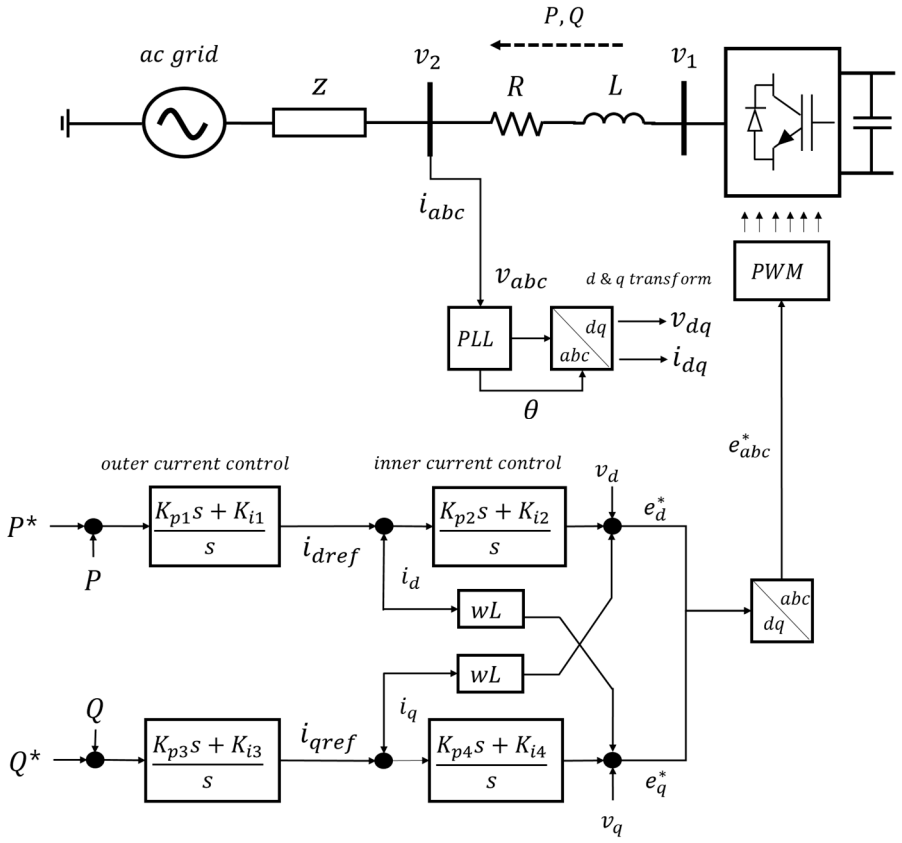

Figure 2. VSC control block diagram. PWM: Pulse With Modulation; PLL Phase-Locked Loop.

The PWM switching delay is then approximated by a first-order Padé approximation as follows:

$$G_{PWM}(s) = \frac{1 - \frac{1.5T_d s}{2}}{1 + \frac{1.5T_d s}{2}}, \tag{6}$$

where T_d is the switching delay in the PWM. Then, combining (5) and (6), the equation can be rearranged by the input terms as v_2^{dq} and $i_{dq,ref}$, with i_{dq} as the output. The transfer functions of the inner controller are expressed by:

$$i_d = A \cdot v_2^d + B \cdot i_{d,ref}, \tag{7}$$

$$i_q = A \cdot v_2^q + B \cdot i_{q,ref}, \tag{8}$$

where $A = \frac{1 - G_{PWM}(s)}{(R+Ls) + G_{PWM}(s) \cdot A_d(s)}$, $B = \frac{G_{PWM}(s) \cdot A(s)}{(R+Ls) + G_{PWM}(s) \cdot A_q(s)}$.

The q-axis current of the *d*-*q* frame is aligned with the AC system phasor based on the PLL, i.e., $i_q = 0$. Thus, the converter admittance is derived as i_{abc}/v_2, which is obtained as follows:

$$Y_{VSC}(s) = \frac{1 - G_{PWM}(s)}{(R + Ls) + G_{PWM}(s) \cdot A_d(s)}. \tag{9}$$

Depending on (9), the d-axis current flowing to the AC grid to control active power is represented in Figure 3. Following the block diagram, the stability between the AC grid and converter can be analyzed based on the initial operating point of the VSC. However, the detailed small signal analysis is not of interest in this paper, and the useful results were given with an impedance-based stability analysis theorem by References [23,24].

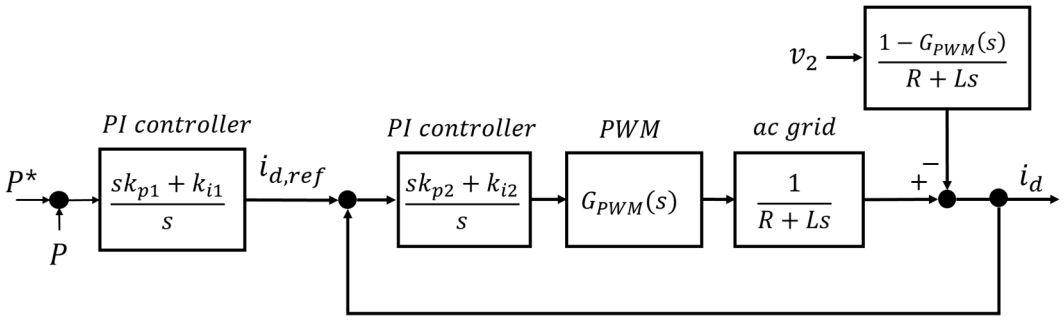

Figure 3. D-axis current control structure of the VSC; PI: Proportional and Integral.

Following the d-axis current response of the converter, the active power of the PGs is simultaneously activated with their own GVIF index. The incremental power of the PGs of area 1 is transferred to area 2, and its characteristic is adjusted by several active power control strategies, as illustrated in the following section.

4. Analysis of Active Power Control Strategies

Excluding the frequency control, two major active power control strategies can be applied for the VSC-HVDC. The first one is the step control, which releases active power step-by-step at certain times, as shown in Figure 4a. The second one is the ramp-rate control, which transfers active power with a specific slope, as illustrated in Figure 4b. In this section, each control strategy is introduced and then defined.

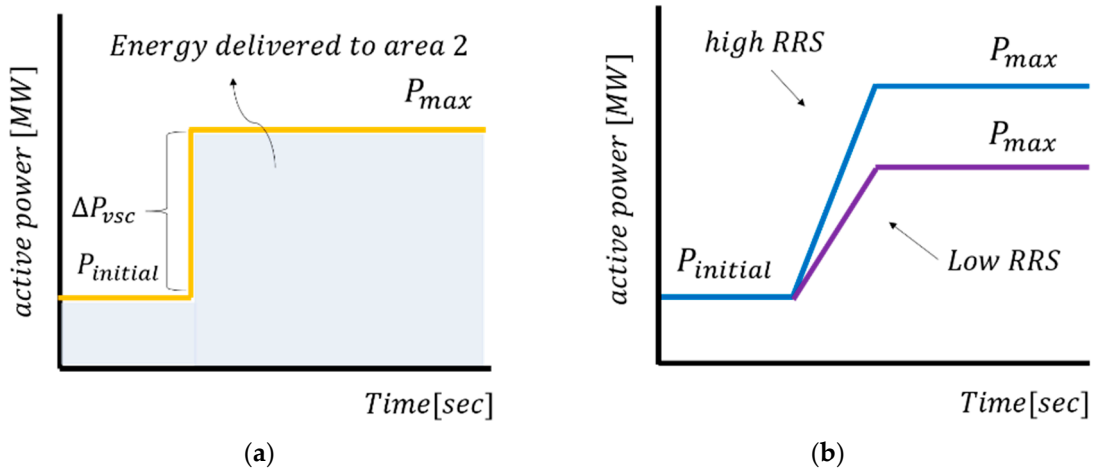

Figure 4. Two major active power control schemes: (**a**) step control (**b**) ramp-rate control with different ramp-rate slopes (RRSs).

4.1. Introduction of Step Control and Ramp-Rate Control Strategies

As is generally known, the step control sustains its initial power in normal stable operation, then increases power at certain times, when area 2 has a frequency drop or emergency event. By contrast, the ramp-rate control has a preset ramp-rate slope (RRS), as shown in Figure 5. The power changes from one stable state to another stable state with a ramping event, and considering a discrete time representation, the ramp-rate of P_{vsc} at the kth instant can be determined using the following expression:

$$RRS = \frac{dP_{vsc}}{dt}(k) = \frac{[P_{vsc}(k) - P_{vsc}(k-1)]}{t(k) - t(k-1)}. \quad (10)$$

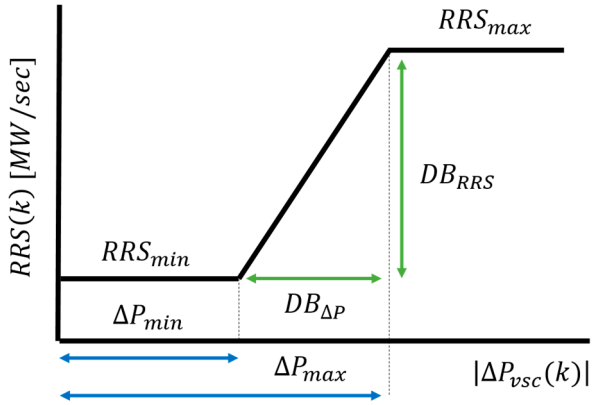

Figure 5. Different RRSs of ramp-rate control; DB: difference between.

The RRS can vary depending upon $|\Delta P_{vsc}(k)|$, which is the absolute value of the deviation between $P_{vsc}(k-1)$ and the active power reference as P_{vsc}^{ref}. If the $|\Delta P_{vsc}(k)|$ is large, a high RRS is applied so as to ensure a fast response. On the other hand, if the power order as P_{vsc}^{ref} is small, a low RRS is applied to follow the final P_{vsc}^{ref} value. Such a droop characteristic is given in Equation (11) with Figure 5.

$$RRS(k) = \begin{cases} RRS_{min},\ if\ |\Delta P_{vsc}(k)| < \Delta P_{min} \\ RRS_{min} + \frac{DB_{RRS}}{DB_{\Delta P}} \times [|\Delta P_{vsc}(k)| - \Delta P_{min}], \\ if\ \Delta P_{min} \le |\Delta P_{vsc}(k)| \le \Delta P_{max} \\ RRS_{max},\ if\ |\Delta P_{vsc}(k)| > \Delta P_{max} \end{cases} . \tag{11}$$

The RRS(k) is a droop-based desired ramp-rate; RRS_{max} and RRS_{min} are the max and min ramp-rate slopes of ΔP_{vsc}, respectively; DB_{RRS} is the difference between and RRS_{max} and RRS_{min}; ΔP_{min} and ΔP_{max} are the lower and upper bands of dynamic change of active power variation; and $DB_{\Delta P}$ is the difference between and ΔP_{min} and ΔP_{max}. As mentioned previously, if the converter receives a high P_{vsc}^{ref} order by the TSO, the active power sharply increases with a ramp rate of RRS_{max}, and a large active power is transferred from area 1 to area 2. Based on References [16,17], it was confirmed that converter power control is helpful when the power system has a contingency event; therefore, this control strategy largely contributes to the frequency stability of area 2. However, we can also expect that the angle stability of area 1 could be further worsened. On the other hand, if the converter reaches RRS_{min} when the $|\Delta P_{vsc}(k)|$ is smaller than ΔP_{min}, a small amount of active power is delivered to area 2, and the angle stability of the PGs in area 1 will be more improved than that in the RRS_{max} case.

4.2. More Detailed Description of Step Control and Ramp-Rate Control Strategies

There is an N-1 contingency event in area 2 with the given scenario, which is represented in Figure 6. Each country, if it has a different Special Protection System (SPS), as the generator tripping schemes are generally called, commonly commands the specific generators to be tripped so as to balance the network power. Basically, the nine cycles as time delay should be taken with the generator tripping scheme, since a mechanical switch is included. As the electronic power equipment only requires communication delay, the activating time is naturally fast [17]. In this paper, three cycles of communication delay are adopted for t_1 time, and the minimum frequency occurred at t_2 time, as shown in Figures 6 and 7. Accordingly, various active power control strategies can be applicable to the VSC-HVDC to supply more power to area 2. Given the frequency fluctuation of area 2, six active power control strategies in total are introduced hereafter.

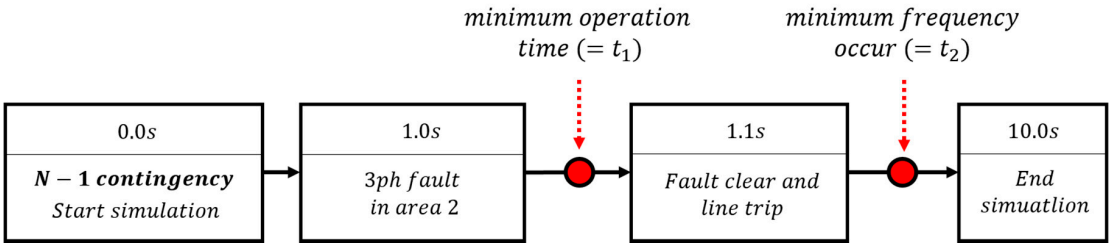

Figure 6. Contingency scenario in area 2.

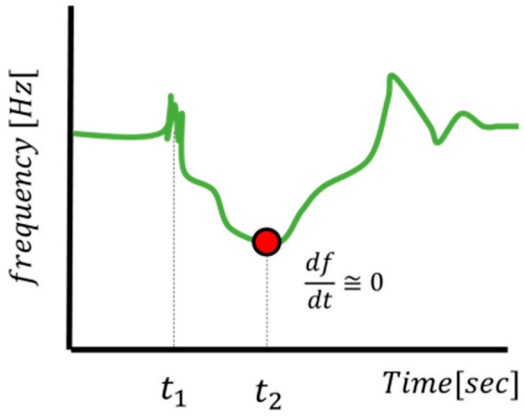

Figure 7. Frequency drop during a contingency event in area 2.

Figure 8a,b both show step control, with the only difference being a power release time. In (a), the power increased at t_1, which is the minimum time to receive an SPS signal as 1.05 s. In (b), the converter changes its power at t_2. Benefiting from the fast response of power electronics, (a) and (b) show advantages of being able to control the power step-by-step, unlike the common generator characteristics. Except for (a) and (b), all other control strategies are ramp-rate control strategies with different RRSs and sending times. Figure 8c,d have different RSSs between t_1 and t_2, which are derived from two different power references. More specifically, the power command in (c) is twice the value of (d); thus, the RRS of (d) is selected to be half. This is to observe the results according to both initial power support speed and amount. Figure 8e,f discuss how the angle stability of each area changed during the recovery stage of area 2. Thus, the two control strategies have the same power reference value, but different RSSs between t_2 and t_3. For this, the t_3 is selected for the control variable to adjust the RSS. In the simulation study, the t_3 of (e) is twice the value of (f), so that (e) has an RRS twice that of (f). According to the control characteristic, the six control schemes are defined in Table 1, and specific simulation results are introduced hereafter.

Table 1. Six different active power control strategies.

Denomination	Control Type	RRS	Control Time
(a)	Step	-	t_1
(b)	Step	-	t_2
(c)	Ramp-rate	RRS_{max}	t_1 to t_2
(d)	Ramp-rate	RRS_{min}	t_1 to t_2
(e)	Ramp-rate	RRS_{max}	t_2 to t_3
(f)	Ramp-rate	RRS_{min}	t_2 to t_3

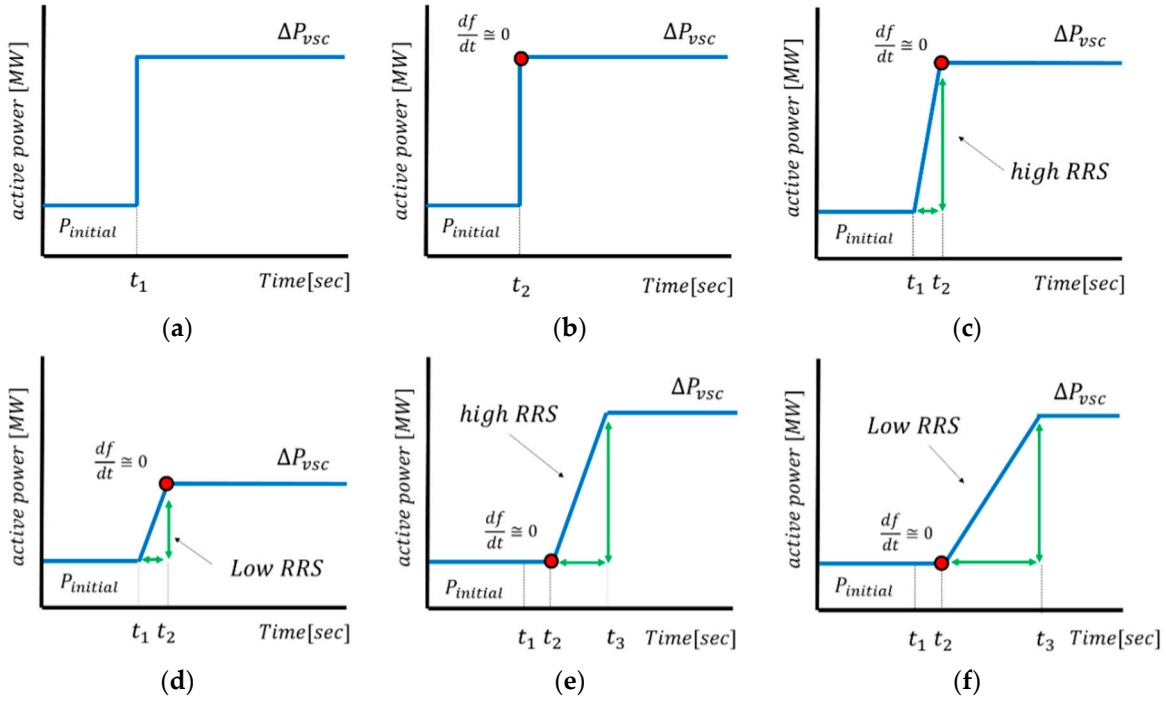

Figure 8. Six active power control schemes: (**a**) step control at t_1; (**b**) step control at t_2; (**c**) ramp-rate control with high RRS between t_1 and t_2; (**d**) ramp-rate control with low RRS between t_1 and t_2; (**e**) ramp-rate control with high RRS between t_2 and t_3; (**f**) ramp-rate control with low RRS between t_2 and t_3.

5. Transient Stability Simulation Results with Six Different Active Power Control Schemes

The interconnected grid configuration for simulation studies is represented in Figure 9, and the three-phase fault event at 345 kV AC transmission occurs in area 2. The detailed system parameters are defined in Table 2. The averaged equivalent circuit of the two-level VSC is used for this feasibility study, and it was supplemented by one on-state switch resistance in each phase, and an equivalent current source at the DC side. Note that the VSC model should be injected by current sources in the PSS®E program, and the outer and inner current controller parameters are adjusted to achieve the desired system response. Accordingly, the six different power output characteristics of the VSC-HVDC are simulated, as shown in Figure 10. There are two power control start times of t_1 and t_2. (a), (c), and (d) supply power at t_1, and (b), (e), and (f) control power at t_2. The RRS and power reference values are all different according to each control characteristic.

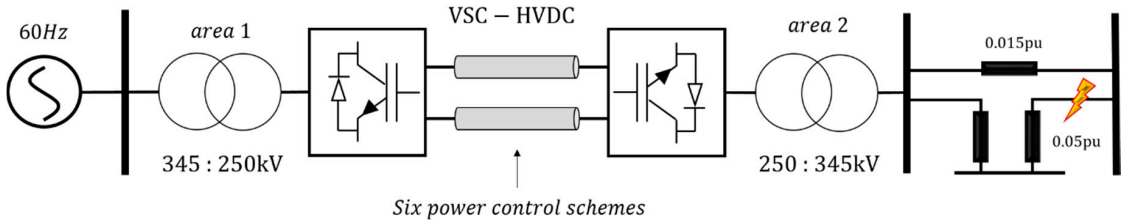

Figure 9. System configuration for simulation studies.

Table 2. System parameters.

Grid Parameters	Value	Converter Parameters	Value
Grid frequency	60 Hz	VSC HVDC Rated capacity	1200 MVA
Total load	94,463 MW	VSC HVDC DC link voltage	250 kV
Total generation	95,802 MW	DC capacitance	1500 μF
AC voltage of each side	345 kV	k_{p1}, k_{p3}	0.5
Short circuit ratio	25	k_{p2}	0.65
Leakage reactance	0.07 pu	k_{p4}	0.8
Transformer Voltage ratio	345/250 250/345	k_{i1}, k_{i3}, k_{i4}	0.01
Transformer rating	1200 MVA	k_{i2}	0.1

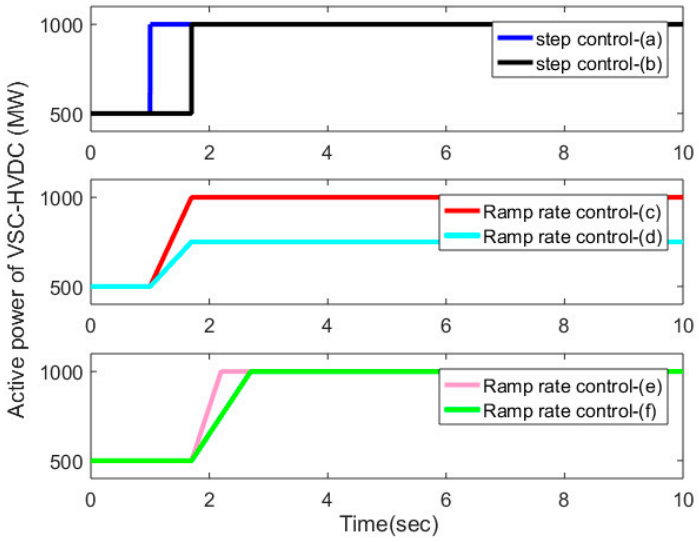

Figure 10. Six power control schemes of the VSC-HVDC.

As mentioned in Section 2, in order to select PGs when the converter controls its power, the GVIF index of the Korean power system is analyzed. The PGs are selected using Equation (3) with ΔP_{vsc} = 100 MW, and the PGs list is given in Table 3. As a total of 269 generators are connected in the Korean grid at the peak load condition; however, for the sake of convenience, only 22 generators with GVIF are illustrated in this paper.

Table 3. Generators-VSC Interaction Factor (GVIF) analysis of participating generators (PGs) in area 1 (ΔP_{vsc} = 100 MW).

Generator Number	Generator List	Initial Power (MW)	GVIF	PGs (O: PG, X: Not PG)
1	Yunghung #G1	800	0.007	O
2	Yunghung #G2	800	0.007	O
3	Yunghung #G3	870	0.01	O
4	Yunghung #G4	870	0.01	O
5	Yunghung #G5	870	0.01	O
6	Yunghung #G6	870	0.01	O
7	Sininchen #G9	167.7	0.004	O
8	Sinin #GT10	167.7	0.004	O
9	Sinin #GT11	168.34	0.003	O
10	Sinin #GT12	168.34	0.003	O

Table 3. *Cont.*

Generator Number	Generator List	Initial Power (MW)	GVIF	PGs (O: PG, X: Not PG)
11	Sininchen #S9	181.26	0	X
12	Inchen #GT1	164.065	0.004	O
13	Inchen #GT3	180.69	0.003	O
14	Inchen #GT5	168	0.005	O
15	Inchen #ST1	163.02	0	X
16	Inchen #ST2	178.12	0	X
17	Inchen #ST3	167.1	0	X
18	POS5 #GT1	210.52	0.005	O
19	POS5#GT2	210.52	0.005	O
20	POS6 #GT3	217.17	0.005	O
21	POS6 #GT4	224.4	0.005	O
22	POS6 #ST2	232.65	0	X
23		⋮		

As can be observed in Table 3, the steam turbine (ST) has a zero value of GVIF, since it has a zero droop value, so the active power is not adjusted in response to the frequency variation. On the other hand, the gas turbine has a certain droop value that is more sensitively activated than the steam turbine during the dynamic converter power control. In order to correct the different frequency measurement results, the GVIF index is used to select PGs. We conclude that the power transmitted to area 2 comes from the generators with GVIF values larger than zero. In addition, as shown in Table 3, the most influential PGs are *Yunghung #G3~#G6* with GVIF = 0.01. With the driven PGs list, the angle spread, which is the difference between the largest and smallest participating machine angles, is analyzed for interconnected areas.

5.1. Angle Spread Evaluation with PGs

In order to evaluate angle spread, the Overcorrections index, which is generally used for control response determination, is introduced in this paper. Assume that $x_{initial}$ is the original steady state value of variable x, x_F is the first encountered peak of x during a transient event, and x_T is the second encountered peak of x during a transient event.

$$x_0 = \left| \frac{x_{initial} - x_F}{x_{initial}} \right| + \left| \frac{x_{initial} - x_T}{x_{initial}} \right| \tag{12}$$

x is defined in this paper as the angle spread. Thus, the larger x_0 is, the worse the angle stability of the PGs, and if x_0 is large enough, there is a possibility of loss of synchronisms. The locus of x_0 as well as the brief conclusions are well illustrated with each scheme hereafter.

5.1.1. Step Control

The results in Figure 11 show the angle spread of two interconnected grids with the control scheme as (a) and (b). Both control schemes are step control strategies, and we aimed to determine whether the active power should be transmitted at t_1 or t_2. In area 1, the only difference between the two schemes is the power release time, so we may see only the result of area 2. From the angle spread results of area 2, it can be seen that sending power at t_2 can further improve the angle stability. More specifically, the first damping of angle spread as x_F after the contingency event is mitigated at about 1.45 s, and the recovery characteristic is more improved from 2.1 s to 3 s. This is because the power from area 1 contributes to the frequency recovery characteristic of area 2. However, in (a), the power is transmitted immediately after the fault, so it contributes less to the angle stability of area 2. The reason for this is that the initial frequency drop driven by fault is momentarily increased due to the immediate active power support. Therefore, the PGs of area 2 generate a relatively small amount

of power according to the small frequency drop. However, this process finally makes a slow frequency recovery, and the angle stability of the PGs becomes worse than that in (b). Therefore, we can conclude that sending power during the frequency recovery stage is more beneficial to both TSOs.

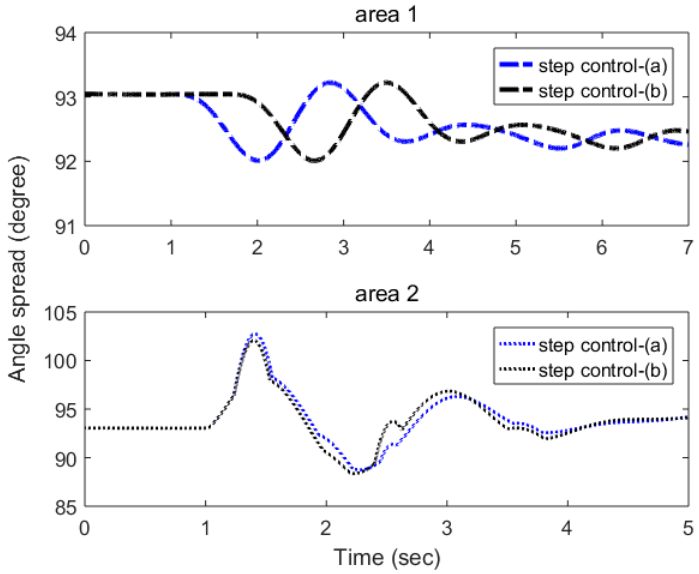

Figure 11. Angle spread results of each area according to (a) and (b) in Table 1.

5.1.2. Ramp-Rate Control

Figure 12 shows the results regarding (c) and (d). Both control schemes are ramp-rate control strategies, and both the RRS between t_1 and t_2 and the active power reference are different. In (c), 1000 MW power is transferred to area 2 with a high RRS, so the angle stability of the sending side is further worsened compared to that in (d), which sends 750 MW. In area 1, (c) experiences a sudden large power change at t_1, and shows a more unstable result. Concerning the receiving side in area 2, the angle deviation x_0 is explicitly different between the two methods. The results show that the generators of area 2 could not cover the severe frequency drop, and there is a possibility of loss of synchronisms at time = 1.45 s. Therefore, applying method (c) is more stable in terms of the angle stability of area 2. However, a tradeoff was observed as method (d) is more suitable for area 1, where the SCR is low.

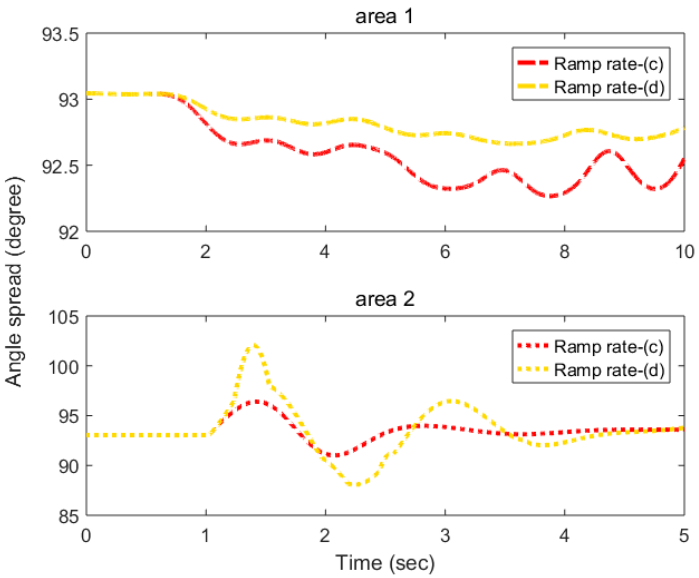

Figure 12. Angle spread results of each area according to (c) and (d) in Table 1.

Figure 13 shows the results regarding (e) and (f). Both control schemes are ramp-rate control strategies, and the only difference is the RRS between t_2 and t_3. The power change references are all the same as 1000 MW; thus, the $|\Delta P_{vsc}(k)|$ is also the same. By adjusting time t_3, the two control methods were set to have a twofold slope difference. Scheme (f), which has a low RRS, shows slightly greater angle stability results in area 1. From the result of area 2, scheme (e) shows a greater angle stability result that the first encountered peak time and its recovery characteristic is faster than that in (f). Thus, it is concluded that active power control with a certain RRS is more suitable for both areas. However, using an overly low RRS will limit the stability improvement of area 2.

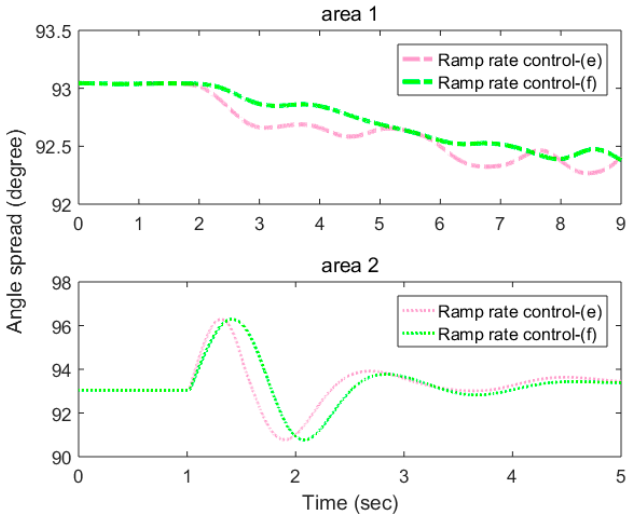

Figure 13. Angle spread results of each area according to (e) and (f) in Table 1.

Figure 14 shows the results regarding (c) and (e). Both control schemes are ramp-rate control strategies with the same RRS, and the only difference is the power sending time. In (c), the power is transmitted immediately following the contingency event (=t_1) while the power is increased during the frequency recovery stage (=t_2) in (e). As shown in the result of area 2, if the grid operator uses both ramp-rate control schemes, sending power during the frequency recovery stage shows more stable results in terms of the angle stability. This is because, as mentioned earlier in Section 5.1.1, the initial frequency drop will not be immediately reduced by (c). This characteristic causes the PGs of area 2 to generate less power. Therefore, at about 1.3 s the first damping angle x_F is more mitigated with (e); thus, sending power at t_2 is more suitable for both TSOs.

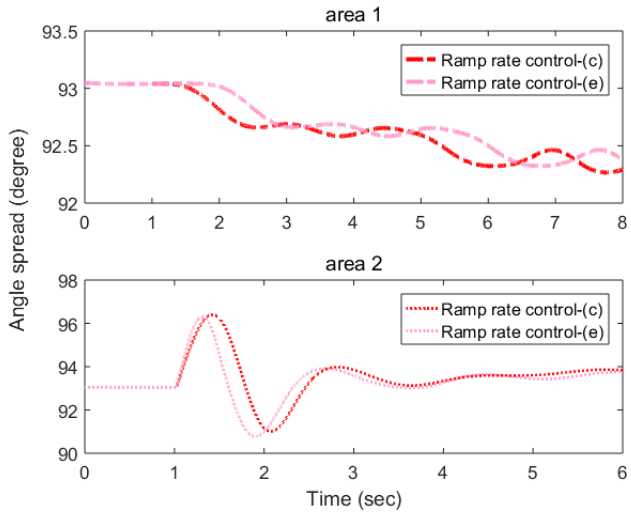

Figure 14. Angle spread results of each area according to (c) and (e) in Table 1.

5.1.3. Step Control vs. Ramp-Rate Control

The results in Figures 15 and 16 are about (a) and (e), and (b) and (e), respectively. The main purpose of this simulation is to compare the step control and ramp-rate control strategies; thus, this comparison is the main result of this paper. The results explicitly show that the angle stability with the step control is more unstable in both areas. Using scheme (e) has more smaller value of x_0 than (a) as shown in Table 4. As a result, the VSC-HVDC connecting two different grids should have its own RRS considering both the sending and receiving side generator stability. Thus, it is recommended that the two TSOs should include the ramp-rate control clauses in the HVDC design phase when the interconnected mutual agreement is introduced.

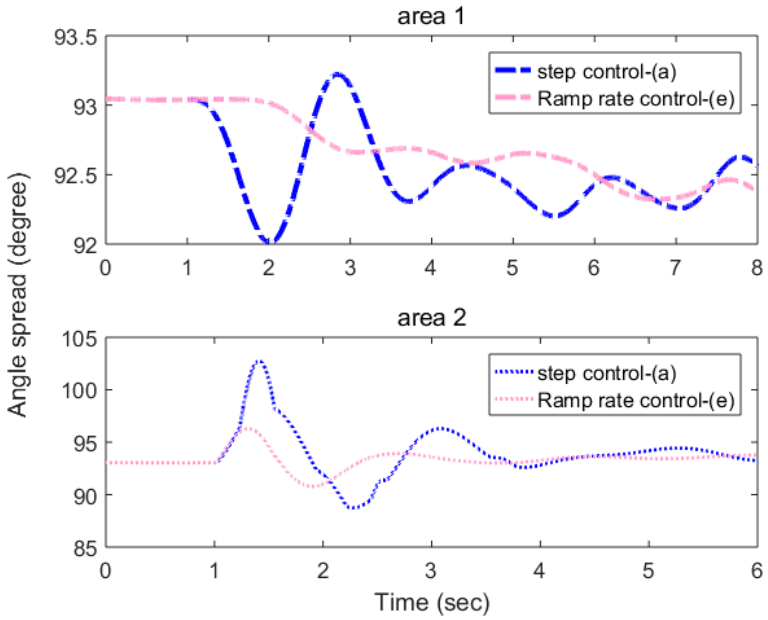

Figure 15. Angle spread results of each area according to (b) and (e).

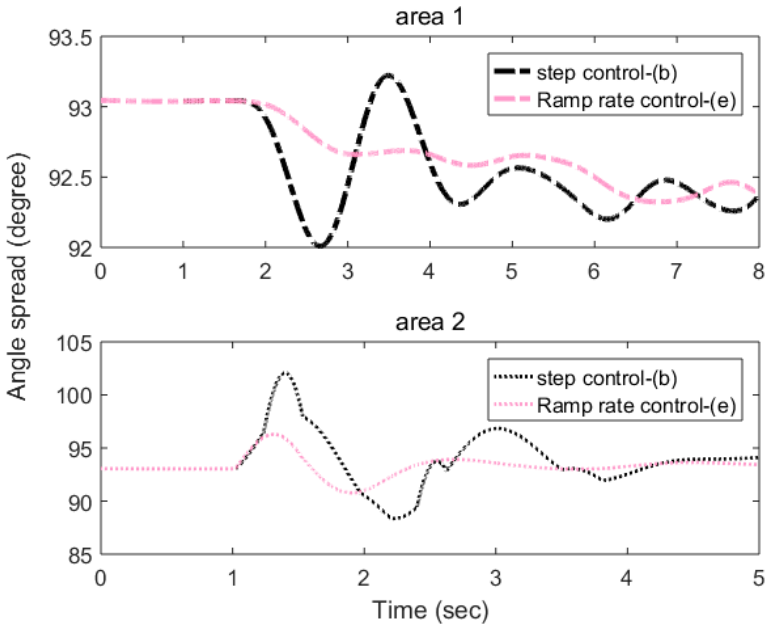

Figure 16. Angle spread results of each area according to (a) and (e).

Table 4. Overcorrection results of (a) and (e) in area 2.

Target System	Control Strategy	$x_{initial}$	x_F	x_T	x_0
area 2	(a)	93.04	102.42	88.6	0.147
	(e)		96.21	90.82	0.05

5.2. Detailed Comparison of Six Power Control Strategies

The suitable control strategy was recommended for each TSO as shown in Table 5. It is confirmed that sending the active power at time t_2 is more effective than that at t_1. This is because the reserve power is helpful during the frequency recovery stage. Furthermore, the ramp-rate control is more suitable than the step control to both areas since the sudden large power change causes the large angle variation of PGs. In addition, the mismatch of active power could further worsen the angle stability, so if the required active power is not estimated, the converter should have its own RRS which is not too far from the generators' output characteristic. Furthermore, if the N-1 or N-2 contingency event occurs at the sending side while the power is transmitted to the receiving side, the ramp-rate control will show a more stable result at the sending side grid. At last, the TSOs should consider the SCR of two grids based on the driven results, and select the appropriate scheme as shown in Table 5. This information will be useful for two TSOs planning grid interconnection projects.

Table 5. Suitable control scheme for each TSO (O: Most suitable/Δ: Suitable/X: Not suitable). SCR: short circuit ratio.

Target System	(a)	(b)	(c)	(d)	(e)	(f)
Receiving side with high SCR	Δ	Δ	O	O	O	O
Receiving side with Low SCR	X	X	O	Δ	O	Δ
Sending side with high SCR	Δ	Δ	O	O	O	O
Sending side with Low SCR	X	X	Δ	O	O	O

6. Conclusions

To date, the frequency control for interconnected grids has been analyzed in several works. However, using frequency control increases the operation burden of one side. Thus, the impact of various types of active power control scheme should be simulated and analyzed. Furthermore, if there is a power increase clause between interconnected grids, this issue will be more critical for grid operators. In this paper, when the receiving side has an emergency event, six applicable active power control strategies are defined and simulated.

Before the simulation, our researchers expected that the step control, which is a powerful strength of power electronics, could further improve the angle stability of PGs due to its fast response. Contrary to expectations, the results show that the VSC-HVDC with certain RRSs similar to the other generator output characteristics provides more stable results in several cases. Our findings also confirm that sending power during the frequency recovery stage is more effective for the receiving side, whereas sending power right after the fault degrades the generator output characteristic since the low initial frequency error is measured at the generator side. To prevent this problem, one solution can be applied. If the droop slope of the generator is adjusted when the converter starts the power control, the small initial frequency error caused by the converter support can be corrected at each governor. This increases the generators output, and thus the frequency can reach the nominal value.

Furthermore, grid operators have to alter their control strategy based on the SCR of each grid base, as shown in Table 5. These results provide useful information to grid operators, and the advantages and disadvantages of each control scheme are well shown.

Author Contributions: The main idea was proposed by S.S. and G.J.; the experiment results were collected and analyzed by S.S. and M.Y.

Funding: This research received no external funding.

Acknowledgments: This work was supported under the framework of international cooperation program managed by National Research Foundation of Korea (No. 2017K1A4A3013579) and also supported by "Human Resources Program in Energy Technology" of the Korea Institute of Energy Technology Evaluation and Planning (KETEP), granted financial resource from the Ministry of Trade, Industry and Energy, Korea. (No. 20174030201540).

Conflicts of Interest: The authors declare no conflict of interest.

Nomenclature

θ	Angle difference between $\dot{E}_1$ and $\dot{E}_2$
$\dot{E}_1$	Internal generators voltage
$\dot{E}_2$	Infinite bus voltage
w	Rotor speed
H	Shaft inertia
P_i	Mechanical power
P_n	Electrical power
v_1	voltage at voltage source converter
v_2	voltage at PCC
R	Resistance between AC grid and converter
L	Inductance between AC grid and converter
i	Ac current from converter to AC grid
k_p, k_i	PI controller in current controller of VSC
T_d	Switching delay in PWM
RRS	Ramp-rate slope of VSC
$\lvert\Delta P_{vsc}(k)\rvert$	Absolute value of the deviation between $P_{vsc}(k-1)$ and active power reference as P_{vsc}^{ref}
x_0	Overcorrections for the evaluation of angle spread

References

1. Yang, D.; Wang, X.; Liu, F.; Xin, K.; Liu, Y.; Blaabjerg, F. Adaptive reactive power control of PV power plants for improved power transfer capability under ultra-weak grid conditions. *IEEE Trans. Smart Grid* **2017**. [CrossRef]
2. Purvins, A.; Wilkening, H.; Fulli, G.; Tzimas, E.; Celli, G.; Mocci, S.; Pilo, F.; Tedde, S. A European supergrid for renewable energy: Local impacts and far-reaching challenges. *J. Clean. Prod.* **2011**, *19*, 1909–1916. [CrossRef]
3. Singh, M.; Khadkikar, V.; Chandra, A.; Varma, R.K. Grid interconnection of renewable energy sources at the distribution level with power-quality improvement features. *IEEE Trans. Power Deliv.* **2011**, *26*, 307–315. [CrossRef]
4. Feltes, J.; Gemmell, B.; Retzmann, D. From smart grid to super grid: Solutions with HVDC and FACTS for grid access of renewable energy sources. In Proceedings of the 2011 IEEE Power and Energy Society General Meeting, Detroit, MI, USA, 24–29 July 2011; pp. 1–6.
5. Entsoe. Agreement Regarding Operation of the Interconnected Nordic Power System (System Operation Agreement). 2006. Available online: https://docstore.entsoe.eu/Documents/Publications/SOC/Nordic/System_Operation_Agreement_2014.pdf (accessed on 1 January 2019).
6. Aljohani, T.M.; Alzahrani, A.M. The Operation of the GCCIA HVDC Project and Its Potential Impacts on the Electric Power Systems of the Region. *Int. J. Electron. Electr. Eng.* **2014**, *2*, 207–213. [CrossRef]
7. Zhang, L.; Harnefors, L.; Nee, H.-P. Interconnection of two very weak AC systems by VSC-HVDC links using power-synchronization control. *IEEE Trans. Power Syst.* **2011**, *26*, 344–355. [CrossRef]
8. Flourentzou, N.; Agelidis, V.G.; Demetriades, G.D. VSC-based HVDC power transmission systems: An overview. *IEEE Trans. Power Electron.* **2009**, *24*, 592–602. [CrossRef]
9. Daryabak, M.; Filizadeh, S.; Jatskevich, J.; Davoudi, A.; Saeedifard, M.; Sood, V.; Martinez, J.; Aliprantis, D.; Cano, J.; Mehrizi-Sani, A. Modeling of LCC-HVDC systems using dynamic phasors. *IEEE Trans. Power Deliv.* **2014**, *29*, 1989–1998. [CrossRef]

10. Huang, Y.; Wang, D. Effect of Control-Loops Interactions on Power Stability Limits of VSC Integrated to AC System. *IEEE Trans. Power Deliv.* **2018**. [CrossRef]
11. Zhou, J.Z.; Ding, H.; Fan, S.; Zhang, Y.; Gole, A.M. Impact of Short-Circuit Ratio and Phase-Locked-Loop Parameters on the Small-Signal Behavior of a VSC-HVDC Converter. *IEEE Trans. Power Deliv.* **2014**, *29*, 2287–2296. [CrossRef]
12. Huang, Y.; Yuan, X.; Hu, J.; Zhou, P. Modeling of VSC connected to weak grid for stability analysis of DC-link voltage control. *IEEE J. Emerg. Sel. Top. Power Electron.* **2015**, *3*, 1193–1204. [CrossRef]
13. Davari, M.; Mohamed, Y.A.-R.I. Robust vector control of a very weak-grid-connected voltage-source converter considering the phase-locked loop dynamics. *IEEE Trans. Power Electron.* **2017**, *32*, 977–994. [CrossRef]
14. Wu, G.; Liang, J.; Zhou, X.; Li, Y.; Egea-Alvarez, A.; Li, G.; Peng, H.; Zhang, X. Analysis and design of vector control for VSC-HVDC connected to weak grids. *CSEE J. Power Energy Syst.* **2017**, *3*, 115–124. [CrossRef]
15. Suul, J.A.; D'Arco, S.; Rodríguez, P.; Molinas, M. Impedance-compensated grid synchronisation for extending the stability range of weak grids with voltage source converters. *IET Gener. Transm. Distrib.* **2016**, *10*, 1315–1326. [CrossRef]
16. Song, S.; Kim, J.; Lee, J.; Jang, G. AC Transmission Emulation Control Strategies for the BTB VSC HVDC System in the Metropolitan Area of Seoul. *Energies* **2017**, *10*, 1143. [CrossRef]
17. Song, S.; Hwang, S.; Ko, B.; Cha, S.; Jang, G. Novel Transient Power Control Schemes for BTB VSCs to Improve Angle Stability. *Appl. Sci.* **2018**, *8*, 1350. [CrossRef]
18. Chaudhuri, N.R.; Chaudhuri, B. Adaptive droop control for effective power sharing in multi-terminal DC (MTDC) grids. *IEEE Trans. Power Syst.* **2013**, *28*, 21–29. [CrossRef]
19. Renedo, J.; Garcia-Cerrada, A.; Rouco, L. Active power control strategies for transient stability enhancement of AC/DC grids with VSC-HVDC multi-terminal systems. *IEEE Trans. Power Syst.* **2016**, *31*, 4595–4604. [CrossRef]
20. Du, C.; Bollen, M.H. Power-frequency control for VSC-HVDC during island operation. In Proceedings of the 8th IEE International Conference on AC-DC Power Transmission, London, UK, 28–31 March 2006.
21. Alamuti, M.M.; Saunders, C.S.; Taylor, G.A. A novel VSC HVDC active power control strategy to improve AC system stability. In Proceedings of the PES General Meeting | Conference & Exposition, National Harbor, MD, USA, 27–31 July 2014; pp. 1–5.
22. Yang, T.; Zhang, Y.; Wang, Z.; Pen, H. Secondary Frequency Stochastic Optimal Control in Independent Microgrids with Virtual Synchronous Generator-Controlled Energy Storage Systems. *Energies* **2018**, *11*, 2388. [CrossRef]
23. Bayo-Salas, A.; Beerten, J.; Rimez, J.; Van Hertem, D. Impedance-based stability assessment of parallel VSC HVDC grid connections. In Proceedings of the 11th IET International Conference on AC and DC Power Transmission, Birmingham, UK, 10–12 February 2015.
24. Wen, B.; Dong, D.; Boroyevich, D.; Burgos, R.; Mattavelli, P.; Shen, Z. Impedance-based analysis of grid-synchronization stability for three-phase paralleled converters. *IEEE Trans. Power Electron.* **2016**, *31*, 26–38. [CrossRef]